Journal of the Serbian Society for Computational Mechanics / Vol. 19 / No. 1, 2025 / pp 185-196 / review paper
(10.24874/jsscm.2025.19.01.10)

TURBULENT FLUID FLOW MODEL WITH APPLICATION IN BIOMEDICINE

Aleksandar Nikolic[1*] [0000-0002-7052-7444], Miroslav Živković[2] [0000-0002-0752-6289], Nenad Filipović [2] [0000-0001-9964-5615], Marko Topalović [1] [0000-0001-6101-755X]

[1] Institute for Information Technologies Kragujevac, University of Kragujevac, Jovana Cvijića bb, 34000 Kragujevac, Serbia.
e-mail: dziga@kg.ac.rs, topalovic@kg.ac.rs.
[2] Faculty of Engineering, University of Kragujevac, Sestre Janjić 6, 34000 Kragujevac, Serbia.
zile@kg.ac.rs, fica@kg.ac.rs.
**corresponding author*

Abstract

Two-equation turbulent models are widely used in finite element analysis of fluid flow. The PAK program package was upgraded from the classical laminar flow to the turbulent k-omega model. The turbulence model was validated using the case of fluid flow in a backward-facing step channel. The analysis results show good agreement with experimental data reported in the literature. The code was subsequently tested on a case of fluid flow in a coronary artery bifurcation, with particular emphasis on the stenosis resulting from the patient's disease.

Keywords: turbulent fluid flow, k-omega model, coronary artery bifurcation, stenoses

1. Introduction

Turbulence in viscous fluid dynamics plays a key role in many engineering applications, as it significantly affects the distribution of pressure, velocity, and shear in fluid systems. When a fluid becomes turbulent, the flow is no longer laminar (regular and smooth), but rather chaotic, swirling flows that generate large fluctuations in their magnitudes occur. This flow is often the result of an increase in fluid velocity or when the fluid passes past solid bodies, such as pipes or surfaces. Turbulent flow is characterized by high energy being transferred from the large-scale flow to the smaller scales (microflows), which leads to higher energy losses and higher friction forces on the surfaces through which the fluid flows (Nikolić, 2018).

There are several approaches to describing and studying turbulent fluid flow. The most common approach is statistical turbulence modeling. This approach relies on the approximation that the fluid velocity can be expressed as the sum of the mean velocity and the fluctuating component around that mean (McDonough, 2007). Applying this decomposition to the Navier–Stokes equations results in the Reynolds-Averaged Navier–Stokes (RANS) equations (Wilcox, 1988). These equations contain mean values of velocity and pressure instead of instantaneous quantities, but also introduce additional terms known as turbulent stresses or Reynolds stresses. The $k-\omega$ model has been successfully applied to predict turbulent flows in the works of

(Wilcox, 1994), (Wilcox, 2006) and (Bassi et al., 2014), (Bassi et al., 2014). However, its application in biomechanical and medical research remains relatively limited.

The development of the turbulence module for fluid flow calculations in this paper is based on the finite element method (FEM) (Bathe, 2006). An implicit integration scheme was employed for solving the governing equations of the problem. The fluid velocity, pressure, turbulence kinetic energy, and turbulence dissipation rate were determined at the finite element nodes through an incremental–iterative procedure, following the approach of (Kojić et al., 2008).

In biomedical research, arteries with narrowing of the cross-section (stenosis) are particularly interesting to study (Shi et al., 2011). Blood flow in arteries is usually characterized as laminar before stenosis, while after stenosis, a vortex flow occurs that can best be characterized as turbulent flow. The study of this phenomenon is also interesting from a medical perspective. After each narrowing and sudden expansion of the cross-section of the artery, there is an accumulation of bad cholesterol that can further develop into atherosclerotic plaque that leads to a heart attack. To accelerate the process of model generation, the STL2FEM software was developed (Blagojević et al., 2013), based on volumetric models obtained from radiological imaging.

A verification example of turbulent flow in a channel with a backward-facing step is presented. Comparison with experimental results from the literature (Jovic, 1994) shows that the FEM analysis corresponds well with the measurements.

2. Methodology

2.1 RANS equations and k-ω model

The Reynolds-Averaged Navier–Stokes (RANS) equations represent the first step in the statistical modeling of turbulence. They are derived from the Navier–Stokes equations and the continuity equation (Kojić et al. 2008):

$$\rho\left[\frac{\partial \overline{v}_i}{\partial t}+\overline{v}_j\frac{\partial \overline{v}_i}{\partial x_j}\right]=-\frac{\partial \overline{p}}{\partial x_i}+\frac{\partial}{\partial x_j}\left[\left(\mu_{eff}\right)\left(\frac{\partial \overline{v}_i}{\partial x_j}+\frac{\partial \overline{v}_j}{\partial x_i}\right)\right] \tag{1}$$

$$\frac{\partial \overline{v}_i}{\partial x_i}=0 \tag{2}$$

where $\mu_{eff}=\mu+\mu_T$ is the effective dynamic viscosity, defined as the sum of the molecular dynamic viscosity and the turbulent (eddy) viscosity.

Equations (1) and (2) represent the Reynolds-Averaged Navier–Stokes (RANS) equations. In the $k-\omega$, the turbulent (eddy) viscosity is calculated as the ratio of the turbulence kinetic energy to the specific dissipation rate of turbulence kinetic energy:

$$\mu_T=\alpha^*\frac{k}{\omega} \tag{3}$$

The turbulence kinetic energy can be expressed, following (McDonough, 2007), by the equation:

$$\rho\left(\frac{\partial k}{\partial t}+\bar{v}_j\frac{\partial k}{\partial x_j}\right)=\frac{\partial}{\partial x_j}\left[\left(\mu+\sigma^*\mu_T\right)\frac{\partial k}{\partial x_j}\right]+P_k-\beta_k\rho k\omega \tag{4}$$

where P_k denotes the effect of turbulence kinetic energy and is defined as:

$$P_k=\mu_T\left(\frac{\partial\overline{v_i}}{\partial x_j}+\frac{\partial\overline{v_j}}{\partial x_i}\right)\frac{\partial\overline{v_i}}{\partial x_j} \tag{5}$$

The specific dissipation rate of turbulence kinetic energy, ω, is a variable that characterizes the turbulence scale and is calculated using the following equation:

$$\rho\left(\frac{\partial\omega}{\partial t}+\bar{v}_j\frac{\partial\omega}{\partial x_j}\right)=\frac{\partial}{\partial x_j}\left[\left(\mu+\sigma\mu_T\right)\frac{\partial\omega}{\partial x_j}\right]+\alpha_k\frac{\omega}{k}P_k-\beta_\omega\rho\omega^2 \tag{6}$$

In equations (4) and (6) contants α^*, α, β_ω, β_k, σ and σ^* are defined following (Wilcox, 1994) and (Wilcox, 2006) as:

$$\alpha^*=1,\quad \alpha_k=\frac{5}{9},\quad \beta_\omega=\frac{3}{40},\quad \beta_k=\frac{9}{100},\quad \sigma=\frac{1}{2},\quad \sigma^*=\frac{1}{2} \tag{7}$$

2.2 Finite element formulation of RANS equations and k-ω model

The basic idea of finite element analysis is to discretize the spatial domain into subdomains called finite elements. Figure 1 schematically illustrates this process using the example of the carotid artery, where the fluid (blood) domain is explicitly modeled. Both domains are subdivided into finite elements, within which the fundamental physical quantities are computed. In the previous chapter, we presented the governing equations for turbulent fluid flow, namely the RANS equations, given by expressions (1) and (2).

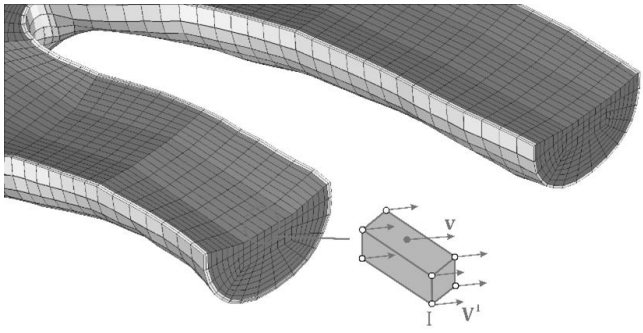

Fig. 1. Discretization of the carotid artery into fluid and solid domains using finite elements

The velocity field within each finite element (Fig. 1) can be approximated by a velocity vector $\mathbf{v}(x,y,z)$, defined in terms of the local coordinates r,s,t of the finite element (Kojić et al., 2008). The finite element velocity is expressed as a function of the nodal velocity vector $\mathbf{v}$ at each node of the element:

$$v_i = \sum_{I=1}^{N} h_I V_i^I \equiv h_I V_i^I, \qquad \mathbf{v} = \mathbf{HV}, \qquad i = 1, 2, 3; \quad I = 1, 2, ..., N \tag{8}$$

where h_k are the interpolation (shape) functions, V_i^I are the components (x, y, z) of the velocity vector at node I and N is the total number of nodes in the finite element.

The governing equations for the [model name] (5–7) can be transformed into finite element balance equations for a single element by applying the standard Galerkin weighting method (Milošević et al., 2018). Specifically, the Galerkin method is applied to equations (1), (2), (5), and (7), using interpolation functions for the fluid velocity, pressure, turbulence kinetic energy, and the specific dissipation rate of turbulence kinetic energy, as described in (Kojić et al., 2008) and (Bathe, 2006):

$$\overline{v}_i = h_{\mathrm{I}} \overline{V_i^{\mathrm{I}}} \tag{9}$$

$$\overline{p}_i = \hat{h}_{\mathrm{I}} P_{\mathrm{I}} \tag{10}$$

$$k = h_{\mathrm{I}} k^{\mathrm{I}} \tag{11}$$

$$\omega = h_{\mathrm{I}} \omega^{\mathrm{I}} \tag{12}$$

The application of this procedure yields the following system of equations in matrix form:

$$\begin{bmatrix} \mathbf{M} & 0 \\ 0 & 0 \end{bmatrix} \begin{bmatrix} \dot{\mathbf{V}} \\ \dot{\mathbf{P}} \end{bmatrix} + \begin{bmatrix} \mathbf{K}_{\mathrm{vv}} + \mathbf{K}_{\mu\mathrm{vt}} & \mathbf{K}_{\mathrm{vp}} \\ \mathbf{K}_{\mathrm{vp}}{}^{\mathrm{T}} & 0 \end{bmatrix} \begin{bmatrix} \mathbf{V} \\ \mathbf{P} \end{bmatrix} = \begin{bmatrix} \mathbf{F}_{\mathrm{v}} + \mathbf{F}_{\mathrm{s}} \\ 0 \end{bmatrix} \tag{13}$$

In previous system submatrices and subvectors are:

$$\left(\overline{\mathbf{M}}\right)_{\mathrm{IJ}} = \rho \int_V h_{\mathrm{I}} h_{\mathrm{J}} dV \tag{14}$$

$$\left(\overline{\mathbf{K}}_{\mathrm{vv}}\right)_{\mathrm{IJ}} = \rho \int_V h_{\mathrm{I}} h_{\mathrm{K}} \overline{V_j}^{\mathrm{I}} h_{\mathrm{J},j} dV \tag{15}$$

$$\left(\overline{\mathbf{K}}_{\mu\mathrm{vt}}\right)_{\mathrm{IJ}} = \int_V \left(\mu + \mu_T\right) h_{\mathrm{I},j} h_{\mathrm{J},j} dV \tag{16}$$

$$\left(\mathbf{K}_{\mathrm{vpi}}\right)_{\mathrm{IJ}} = -\int_V h_{\mathrm{I},i} \hat{h}_{\mathrm{J}} dV \tag{17}$$

$$\left(\mathbf{F}_{\mathrm{vi}}\right)_{\mathrm{I}} = \rho \int_V h_{\mathrm{I}} f_i^V dV \tag{18}$$

$$\left(\mathbf{F}_{\mathrm{si}}\right)_{\mathrm{I}} = \int_S h_{\mathrm{I}} \left[-\overline{p} n_i + \left(\mu + \mu_T\right) \overline{V_{i,j}}^{\mathrm{I}} n_j \right] dS \tag{19}$$

For the turbulence model $k-\omega$, the finite element equations are derived from equations (4) and (6), and can be formulated as:

$$\left[\mathbf{M_K}\right]\left[\dot{\mathbf{k}}\right]+\left[\mathbf{K_{VK}}+\mathbf{K_{MK}}+\mathbf{K_{\beta k}}\right]\left[\mathbf{k}\right]-\left[\mathbf{K_{VV1}}\right]\left[\mathbf{V}\right]=\mathbf{F_{SK2}} \tag{20}$$

$$\left[\mathbf{M_K}\right]\left[\dot{\boldsymbol{\omega}}\right]+\left[\mathbf{K_{VK}}+\mathbf{K_{M\omega}}+\mathbf{K_{\beta\omega}}\right]\left[\boldsymbol{\omega}\right]-\left[\mathbf{K_{VV2}}\right]\left[\mathbf{V}\right]=\mathbf{F_{S\omega}} \tag{21}$$

In previous equation (20) submatrices and subvectors are:

$$\left(\mathbf{M_K}\right)_{\mathrm{IJ}}=\rho\int_V h_{\mathrm{I}}h_{\mathrm{J}}dV \tag{22}$$

$$\left(\mathbf{K_{VK}}\right)_{\mathrm{IJ}}=\rho\int_V h_{\mathrm{I}}h_{\mathrm{J}}\overline{V_i^{\mathrm{J}}}h_{\mathrm{I},j}dV \tag{23}$$

$$\left(\mathbf{K_{MK}}\right)_{\mathrm{IJ}}=\int_V\left(\mu+\sigma^*\mu_T\right)h_{\mathrm{I},j}h_{\mathrm{J},j}dV \tag{24}$$

$$\left(\mathbf{K_{\beta k}}\right)_{\mathrm{IJ}}=\rho\beta_k\theta\int_V h_{\mathrm{I}}h_{\mathrm{J}}h_{\mathrm{K}}k^{\mathrm{J}}dV \tag{25}$$

$$\left(\mathbf{K_{VV1}}\right)_{\mathrm{IJ}}=2\int_V\mu_T h_{\mathrm{I}}h_{\mathrm{J},j}\overline{V_i^{\mathrm{J}}}h_{\mathrm{K},j}dV \tag{26}$$

$$\left(\mathbf{F_{SK2}}\right)_{\mathrm{I}}=\left(\mu+\sigma^*\mu_T\right)\int_S h_{\mathrm{I}}k_{,j}n_j dS \tag{27}$$

In previous equation (21) submatrices and subvectors are:

$$\left(\mathbf{K_{M\omega}}\right)_{\mathrm{IJ}}=\left[\int_V\left(\mu+\sigma\mu_T\right)h_{\mathrm{I},j}h_{\mathrm{J},j}dV\right] \tag{28}$$

$$\left(\mathbf{K_{\beta\omega}}\right)_{\mathrm{IJ}}=\rho\beta_\omega\int_V h_{\mathrm{I}}h_{\mathrm{J}}h_{\mathrm{K}}\omega^{\mathrm{J}}dV \tag{29}$$

$$\left(\mathbf{K_{VV2}}\right)_{\mathrm{IJ}}=2\alpha_k\theta\mu_T\int_V h_{\mathrm{I}}h_{\mathrm{J},j}\overline{V_i^{\mathrm{J}}}h_{\mathrm{K},j}dV \tag{30}$$

$$\left(\mathbf{F_{S\omega}}\right)_{\mathrm{I}}=\left(\mu+\sigma\mu_T\right)\int_S h_{\mathrm{I}}\omega_{,j}n_j dS \tag{31}$$

By coupling the Reynolds equations (13) with equations (20) and (21), the following system of matrix equations is obtained, based on the works of (Nikolić, 2018) and (Nikolić et al., 2021):

$$\begin{bmatrix}\mathbf{M_V}&0&0&0\\0&0&0&0\\0&0&\mathbf{M_K}&0\\0&0&0&\mathbf{M_K}\end{bmatrix}\begin{bmatrix}\dot{\mathbf{V}}\\\dot{\mathbf{P}}\\\dot{\mathbf{k}}\\\dot{\boldsymbol{\omega}}\end{bmatrix}+\begin{bmatrix}\mathbf{K_{vv}}+\mathbf{K}_{\mu\mathrm{vt}}&\mathbf{K_{vp}}&0&0\\\mathbf{K_{vp}}^{\mathrm{T}}&0&0&0\\-\mathbf{K_{VV1}}&0&\mathbf{K_{VK}}+\mathbf{K_{MK}}+\mathbf{K_{\beta k}}&0\\-\mathbf{K_{VV2}}&0&0&\mathbf{K_{VK}}+\mathbf{K_{M\omega}}+\mathbf{K_{\beta\omega}}\end{bmatrix}\begin{bmatrix}\mathbf{V}\\\mathbf{P}\\\mathbf{k}\\\boldsymbol{\omega}\end{bmatrix}=\begin{bmatrix}\mathbf{F_v}+\mathbf{F_s}\\0\\\mathbf{F_{SK2}}\\\mathbf{F_{S\omega}}\end{bmatrix} \tag{32}$$

All of above procedures and equations are implemented in software PAK-F, part of software package PAK (M. Kojić et al. 1998-2010), which is called PAK-F turbulent.

2.3 Incremental-iterative method for solving equations

The system of equations (13) is nonlinear due to the velocity terms appearing in the convection component. To solve these equations, an incremental–iterative procedure is employed (Kojić et al., 2008). The turbulence kinetic energy, the specific dissipation rate of turbulence kinetic energy, and the fluid velocity at the end of a time step ($t+\Delta t$) bare calculated as the sum of the values from the previous iteration ($i-1$) and the corresponding increment from the current iteration (i). This yields the following iterative equations:

$$\begin{bmatrix} \frac{1}{\Delta t}\mathbf{M}_{\mathrm{v}} + {}^{t+\Delta t}\mathbf{K}_{\mathrm{vv}}{}^{(i-1)} + {}^{t+\Delta t}\mathbf{K}_{\mu\mathrm{vt}}{}^{(i-1)} + {}^{t+\Delta t}\mathbf{J}_{\mathrm{vv}}{}^{(i-1)} & \mathbf{K}_{\mathrm{vp}} \\ \mathbf{K}_{\mathrm{vp}}{}^{T} & 0 \end{bmatrix} \begin{Bmatrix} \Delta\mathbf{V}^{(i)} \\ \Delta\mathbf{P}^{(i)} \end{Bmatrix} = \begin{Bmatrix} {}^{t+\Delta t}\mathbf{F}_{\mathbf{B}}{}^{(i-1)} \\ {}^{t+\Delta t}\mathbf{F}_{\mathbf{P}}{}^{(i-1)} \end{Bmatrix} \tag{33}$$

Equations (20) and (21) in incremental-iterative matrix expressions can be written as:

$$\begin{bmatrix} 0 & 0 & 0 \\ {}^{t+\Delta t}\mathbf{K}_{\mathrm{KV}}{}^{(i-1)} + {}^{t+\Delta t}\mathbf{K}_{\mathrm{VVK}}{}^{(i-1)} & \frac{1}{\Delta t}\mathbf{M}_{\mathrm{K}} + {}^{t+\Delta t}\mathbf{K}_{\mathrm{VK}}{}^{(i-1)} + {}^{t+\Delta t}\mathbf{K}_{\mathrm{MK}}{}^{(i-1)} + {}^{t+\Delta t}\mathbf{K}_{\beta\mathrm{k}}{}^{(i-1)} & 0 \\ + {}^{t+\Delta t}\mathbf{K}_{\omega\mathrm{V}}{}^{(i-1)} + {}^{t+\Delta t}\mathbf{K}_{\mathrm{VV}\omega}{}^{(i-1)} & 0 & \frac{1}{\Delta t}\mathbf{M}_{\mathrm{K}} + {}^{t+\Delta t}\mathbf{K}_{\mathrm{VK}}{}^{(i-1)} + {}^{t+\Delta t}\mathbf{K}_{\mathrm{M}\omega}{}^{(i-1)} + {}^{t+\Delta t}\mathbf{K}_{\beta\omega}{}^{(i-1)} \end{bmatrix} \begin{Bmatrix} \Delta\mathbf{V}^{(i)} \\ \Delta\mathbf{k}^{(i)} \\ \Delta\boldsymbol{\omega}^{(i)} \end{Bmatrix} = \begin{Bmatrix} {}^{t+\Delta t}\mathbf{R}_{\mathrm{V}}{}^{(i-1)} \\ {}^{t+\Delta t}\mathbf{R}_{\mathrm{K}}{}^{(i-1)} \\ {}^{t+\Delta t}\mathbf{R}_{\omega}{}^{(i-1)} \end{Bmatrix} \tag{34}$$

3. Verification and examples of turbulent fluid flow with k-omega model

3.1 Example with backward-facing step

The turbulence module was validated using a widely adopted benchmark problem—the flow over a backward-facing step. The geometry of the problem, given in (Jović et al., 1994), is shown in Fig. 2.

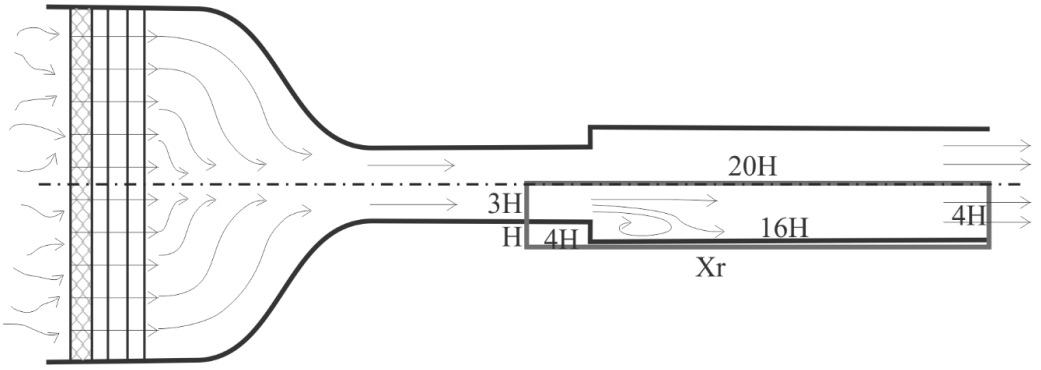

Fig. 2. Geometry of a backward-facing step model

In this model, the sudden expansion of the tunnel cross-section generates a vortex behind the step, as illustrated in Fig. 2. The upstream section of the tunnel, which serves to establish a laminar flow regime prior to the step, is not included in the analysis. Owing to symmetry

conditions, only half of the tunnel with the step, highlighted by the red rectangle in Fig. 2, is modeled.

The step has a relative height H, and its relative length is *4H*. The total length of the modeled tunnel section is *20H*. The result considered in this problem is the distance after which the fluid falls to the bottom of the channel, denoted by *Xr* on Fig. 2. Dimension X_r has been experimentally determined as 6H. Inside the tunnel is a Newtonian fluid of density $\rho = 1e^{-3} g/mm^3$ with dynamic viscosity $\mu = 1e^{-2} g/mms$. The problem is simulated with multiple inlet velocities, with emphasis on velocities where the Reynolds number is greater than 2300 and turbulent flow occurs. At an inlet average fluid velocity of $v_{inlet} = 16666 mm/s$ a Reynolds number of 5000 is obtained.

The boundary conditions in the model prescribe a no-slip condition (v=0) on the channel walls, while zero surface forces are imposed at the channel outlet. The upper boundary of the model is simulated as symmetrical because the model practically represents half of the tunnel. A model with 28,000 four-node elements was used for the calculation, as represented in Fig. 3.

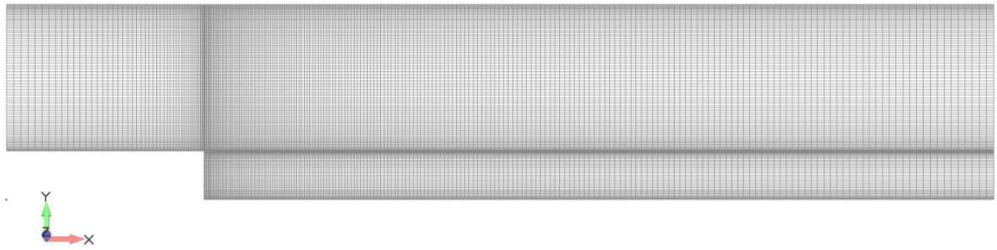

Fig. 3. Finite element model of the 2D backward-facing step channel with a 28,000-element mesh

The inlet boundary conditions were defined by the average velocity v_{inlet}, turbulence kinetic energy k_0 and specific dissipation rate of turbulence kinetic energy ω_0, calculated following (Nikolić, 2018) and (Nikolić et al., 2021). Wall boundary conditions for the turbulence quantities k and ω were imposed according to the formulations given in (Nikolić, 2018). At the outlet, the pressure was set to zero. The FEM simulation of fluid flow in the stepped channel using the *k-ω* turbulence model was implemented as a transient (non-stationary) analysis. The computation was carried out over 200 time steps of 0.5 seconds each, using a mesh of 28,000 elements. The results obtained with the PAK-F Turbulent software were compared with available experimental data for the characteristic reattachment lengths X_r (2H,4H and 6H), as shown in Fig. 5.

The length $X_r = 0$ corresponds to the end of the step. At a distance $6H$ downstream of the step, the fluid velocity becomes positive, whereas immediately behind the step the velocity in the lower part of the channel is negative (Figure 2). This behavior is caused by the vortex that forms just after the step, where the fluid locally flows in the direction opposite to the inlet velocity. The results in Fig. 4 show the calculated flow field represented by streamlines, obtained with the PAK-F Turbulent program at the beginning of the simulation (t=1s), when the vortex is formed behind the step.

Fig. 4. Streamlines of velocity calculated in software *PAK-F Turbulent*

In the diagrams, the fluid velocity is normalized such that U denotes the local velocity at the observed point, while U_0 represents the average inlet velocity. The computed velocities are thus expressed in dimensionless form relative to the inlet velocity, and the Y-coordinate of each observation point is normalized by the step height H.

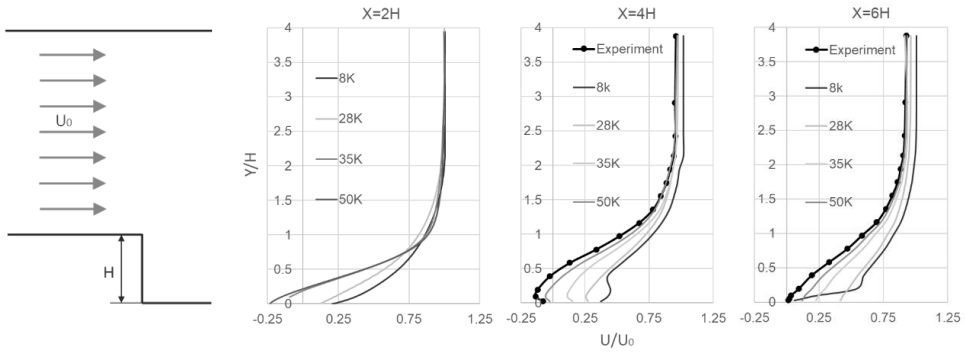

Fig. 5. Results of the 2D backward-facing step analysis at characteristic lengths 2H, 4H and 6H

3.2 Numerical simulation of turbulent flow on the example of a coronary artery bifurcation with large stenosis

The turbulent blood flow was simulated in a coronary artery bifurcation model to investigate hemodynamic conditions under pathological stenosis. A large stenosis model was performed using the real geometry of a selected patient. The FEM model of the fluid domain was modeled with 22674 3D elements, (Fig. 6). The maximum time-averaged inlet blood flow velocity in the coronary artery is $v_{sr} = 3000 mm/s$. The simulation incorporated one full cardiac cycle (systole and diastole) of an adult human, prescribed as a time-dependent boundary condition (Nikolić et al., 2021).

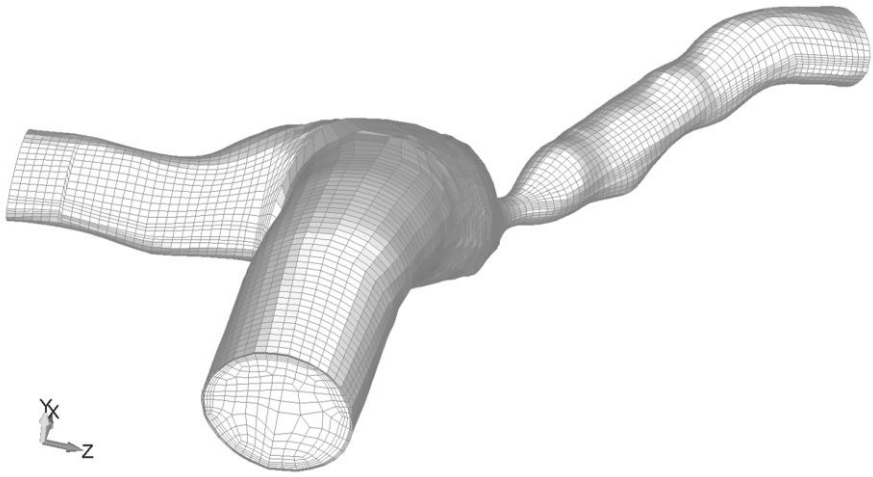

Fig. 6. Finite element model of the coronary artery bifurcation with large stenosis

The boundary conditions for the simulation were defined as follows: zero velocity at the vessel walls (no-slip condition), and resistive boundary conditions at the outlets of the branches to account for the continuation of blood flow into downstream vascular beds. The calculation was performed as an unsteady flow simulation over 200 time steps of 0.005 s each. The results of the blood flow simulation are presented in terms of the velocity field (Figs.7 and 8) and the wall shear stress distribution (Figs. 9 and 10) at several time steps, with particular emphasis on step 20, corresponding to peak systole. The velocity distribution is visualized using streamlines to highlight flow disturbances. The results demonstrate a significant reduction in blood flow velocity within the bifurcation, caused by the severe stenosis located on the main branch of the right coronary bifurcation. In this region, the velocity drops below $v = 1000 mm/s$. The wall shear stress results confirm this behavior, showing stress levels between $800 Pa$ and $900 Pa$. In practice, the shear stress in the stenotic region is up to an order of magnitude higher than in regions without stenosis.

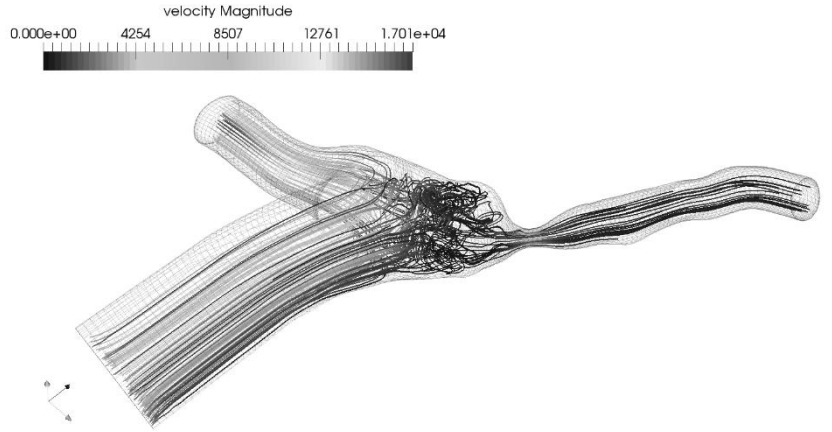

Fig 7. Velocity field in the coronary bifurcation at step 20, illustrating flow during peak systole, (front view).

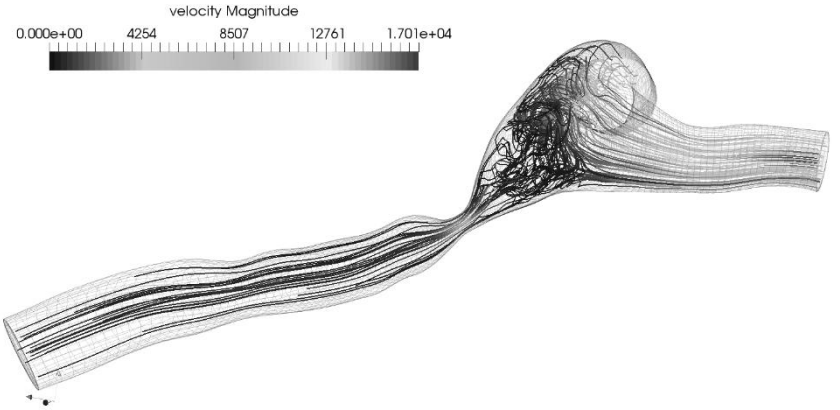

Fig 8. Velocity field in the coronary bifurcation at step 20, illustrating flow during peak systole (back view).

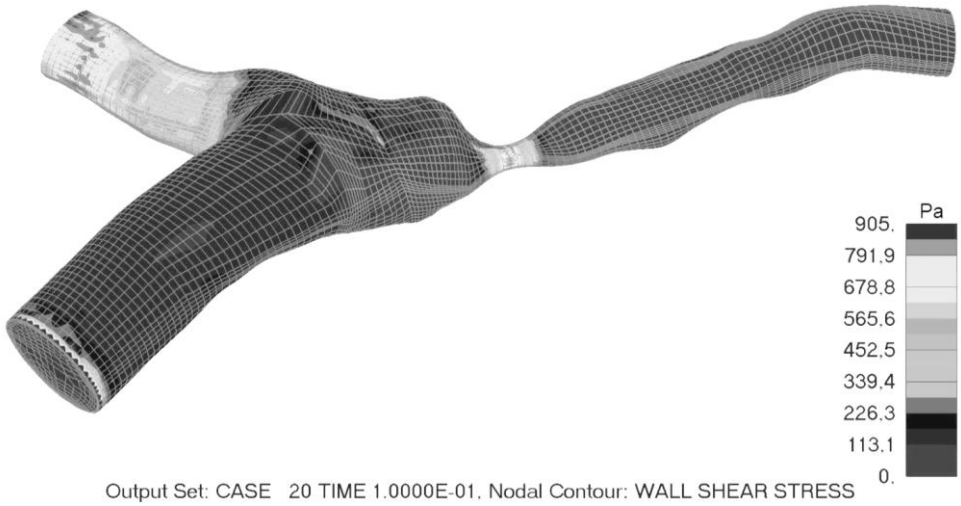

Fig 9. Distribution of wall shear stress the stenosis of coronary artery bifurcation for step 20, (front view).

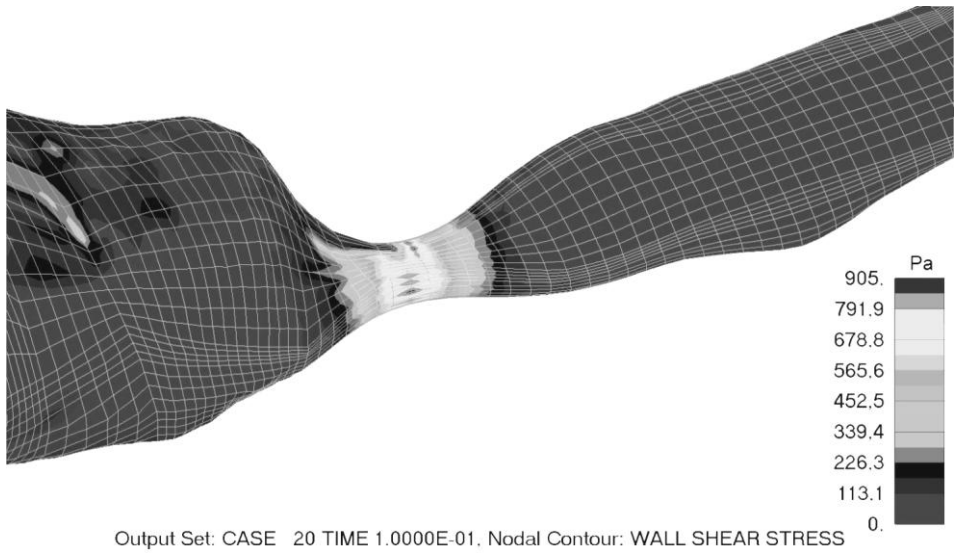

Fig 10. Distribution of wall shear stress in the stenosis of coronary artery bifurcation for step 20, (zoomed view).

4. Conclusions

The sudden narrowing of an artery caused by atherosclerotic plaques triggers biological and mechanical processes that influence the progression of atherosclerosis. Turbulent flow that develops downstream of a stenosis disrupts normal hemodynamics and promotes the accumulation of low-density lipoprotein (LDL) cholesterol and other lipids on the arterial walls. In addition to impairing efficient blood transport, turbulence alters the balance between lipid deposition and removal, accelerating plaque formation. Over time, cholesterol, calcium, and

connective tissue accumulate, producing rigid plaques that further narrow the arteries and obstruct blood flow. In advanced stages, plaque rupture or erosion can occur, leading to thrombus formation, arterial occlusion, and acute cardiovascular events such as myocardial infarction or stroke.

The study of arterial blood flow, particularly transitions from laminar to turbulent regimes, is therefore of great clinical relevance. Flow disturbances caused by stenosis and turbulence can serve as indicators of atherosclerosis and other cardiovascular diseases. Early detection of these changes provides an opportunity to prevent severe outcomes, including heart attack and stroke.

Acknowledgements: The authors acknowledge support of the Ministry of Science of Serbia, grants 451-03-68/2022-14/200378 and TR32036.

References

Nikolić A. *Simulation of laminar and turbulent flow on a realistic model of arterial bifurcation with stenoses*, Doctoral thesis, University of Kragujevac, Serbia, 2018.

Nikolić A, Topalović M, Simić V, Filipović N, Turbulent finite element model applied for blood flow calculation in arterial bifurcation, *Computer Methods and Programs in Biomedicine*, vol. 209, 106328, DOI:10.1016/j.cmpb.2021.106328, (2021).

McDonough J M. *Introductory Lectures on Turbulence, Physics, Mathematics and Modeling*, Departments of Mechanical Engineering and Mathematics, University of Kentucky, 2007.

Wilcox D C. Reassessment of the scale-determining equation for advanced turbulence models, *AIAA Journal*, vol. 26, no. 11, 1299-1310, 1988.

Wilcox D C. *Turbulence Modeling for CFD*, DCW Industries, Inc., 1994.

Wilcox D C. *Turbulence Modeling for CFD, 3rd edition*, La Canada, CA, DCW Industries, Inc., 2006.

Bassi F, Crivellini A, Rebay S and Savini M. Discontinuous Galerkin solution of the Reynolds-averaged Navier–Stokes and k–w turbulence model equations, *Computers & Fluids*, vol. 34, 507–540, 2005.

Bassi F, Ghidoni A, Perbellini A, Rebay S, Crivellini A, Franchina N and Savini M. A high-order Discontinuous Galerkin solver for the incompressible RANS and k–w turbulence model equations, *Computers & Fluids*, vol. 98, 54–68, 2014.

Bathe K J. *Finite Element Procedures, 2nd ed*., Klaus-Jurgen Bathe, 2006.

Blagojević M, Nikolić A, Živković M, Stanković G and Živković M. Influence of block's topologies on endothelial shear stress observed in cfd analysis of artery bifurcation, *Acta of Bioengineering and Biomechanics*, vol. 15, no. 1, 97-104, 2013.

Kojić M, Filipović N, Stojanović B and Kojić N. *Computer Modeling in Bioengineering*, Chichester: John Wiley & Sons Ltd, 2008.

Kojić M, Slavković R, Živković M, Grujović N, Filipović N. *PAK - FE Software for structural analysis, field problems, multiphysics and biomechanics*. Kragujevac, Faculty of Mechanical Engineering, University of Kragujevac, Serbia, (1998/2010)

Milosevic M, Simic V, Milicevic B, Koay E, Ferrari M, Ziemys A and Kojic M. Correction function for accuracy improvement of the Composite Smeared Finite Element for diffusive transport in biological tissue systems, *Computer Methods in Applied Mechanics and Engineering*, vol. 338, 97-116, 2018.

Jovic S and Driver D M. *Backward-facing step measurements at low reynolds number Reh=5000*, NASA Technical Memorandum 108807, 1994.

Shi Y, Lawford P and Hose R, Review of Zero-D and 1-D Models of Blood Flow in the Cardiovascular System, *Biomed. Eng.*, vol. 10, no. 33, 2011.